ACS Photonics

Letter

pubs.acs.org/journal/apchd5

Tyndall Windows: Tunable Scattering of Disordered Solid−Liquid Matching Mixtures

Benedikt Groever,[†] Barmak Heshmat,*[,‡] and Ramesh Raskar[‡]

[†]Harvard School of Engineering and Applied Sciences, Harvard University, Cambridge, Massachusetts, United States

[‡]Media Lab, Massachusetts Institute of Technology, Cambridge, Massachusetts, United States

Supporting Information

ABSTRACT: We explain and explore sharp optical diffusion modulations of solid−liquid matching mixtures. The technique is based on sole refractive index modulation mismatch of optically matching materials at different states. This enables basic materials such as glass-based mixtures to obtain a sharp window of transparency at a desired condition. Our demonstration indicates over 3 orders of magnitude optical transmission modulation with 0.03 thermally induced modulation of the refractive index mismatch. The narrow full width at half maximum of this diffusion modulation is the result of Tyndall scattering of densely packed irregular particles that is not fully explainable by Mie theory. Such mixtures can be used as tunable phantoms and have applications in optofluidics, rheology, and cytometry.

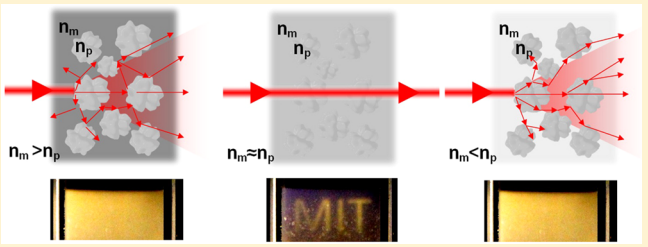

KEYWORDS: *optical materials, disordered photonics, optical diffusion, optical scattering, micro-optics*

Modulation of optical scattering and diffusion is essential in sensing, optical switching, smart glasses, and disordered photonics.[1] Such modulations are realized typically in the solid phase through photochromics,[2] photorefractivity,[3] electrochromics,[4] thermochromics,[5] electrophoretic effects,[6] and liquid crystals.[7] The majority of these effects depends on the photochemical transitions of the material.[8−11] This has raised the quest for engineering better and more efficient materials in expressing these effects since these effects are strongly desired in a broad range of applications all the way from optical processing to imaging and displays.[3−7]

In this work, we propose to use refractive index modulation mismatch of materials at different states to tune the scattering and thus optical diffusion of the entire medium. We demonstrate this tunability with a set of solid−liquid matching mixtures. The results show a window of transparency near the matching region sharper than what is predicted by Mie theory. The work further discusses and assesses the dynamics of cascaded Tyndall scatterings that cause such effects. These mixtures are appealing for a variety of applications in rheology,[12,13] optofluidics,[14,15] cytometry calibration,[16] and realizing tunable tissue phantoms. Our demonstration pronounces and exploits the difference in thermal refractive index change of solids and liquids. However, the same technique can be extended to use any other effect that changes the refractive index of liquids and solids (e.g., electro-optical effects and photorefractive effects). This dichotomy of optical properties in solids and liquids provides a new platform for engineering solid−liquid photonic devices with enhanced performance and functionality.

Scattering from solid particles depends strongly on the hosting environment. While optical liquids (liquids with larger than water refractive index and broadband transparency) are widely used in microscopy for matching the sample medium, reducing aberration, and coupling losses,[17] they have not been used as tuning agents for optical scattering. If a set of nonabsorbing solid particles are submerged in a host optical liquid, the particles will scatter light based on the Radiative Transfer Equation (RTE), which describes light propagation in the most general case.[18] This equation reduces to an optical diffusion equation if the reduced scattering coefficient (the scattering coefficient after considering anisotropy) is much larger than the absorption coefficient $\mu'_s \gg \mu_a$.[19] By modulating the scattering coefficient via an external factor (such as optical absorption or temperature change in our case), the medium can be switched from transparent to diffusive and vice versa for a constant particle density, as in Figure 1a−c. When the temperature of a solid−liquid mixture is changed, the mismatch between the refractive index of liquid (n_m) and solid (n_p) will pass zero due to the mismatch between temperature dependent refractive index gradients of the two different material phases. The temperature dependent variations of the refractive index for liquids are usually much larger than the solids.[20] We call this matching neighborhood the Tyndall window since the particles in a mixture are not exactly spherical Mie particles but, rather, irregular Tyndall particles.

To mathematically frame such behavior we started our model based on Mie theory. At the matching neighborhood the

Received: March 18, 2016
Published: May 23, 2016

DOI: 10.1021/acsphotonics.6b00199
ACS Photonics 2016, 3, 930−935

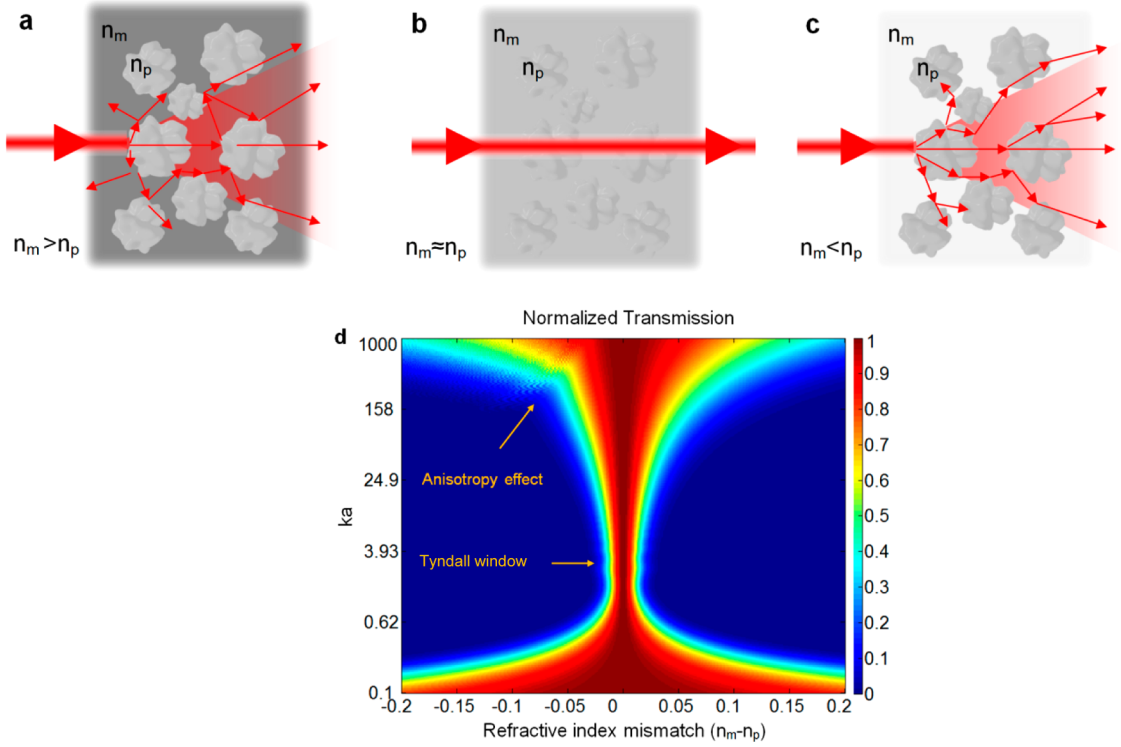

Figure 1. Tyndall windows. (a) Refractive index of particles is less than hosting liquid and, thus, the solid–liquid mixture is diffusive. (b) Mixture passes through a window of transparency (Tyndall window). (c) Mixture becomes diffusive again as liquid refractive index is reduced with increase in temperature. (d) Scattering efficiency of Mie particles predicts the presence of such window in transmission ratio (dark red region). The window has a waist around ka = 3.14; also, scattering anisotropy induces stronger distortion in transmission at larger particle sizes.

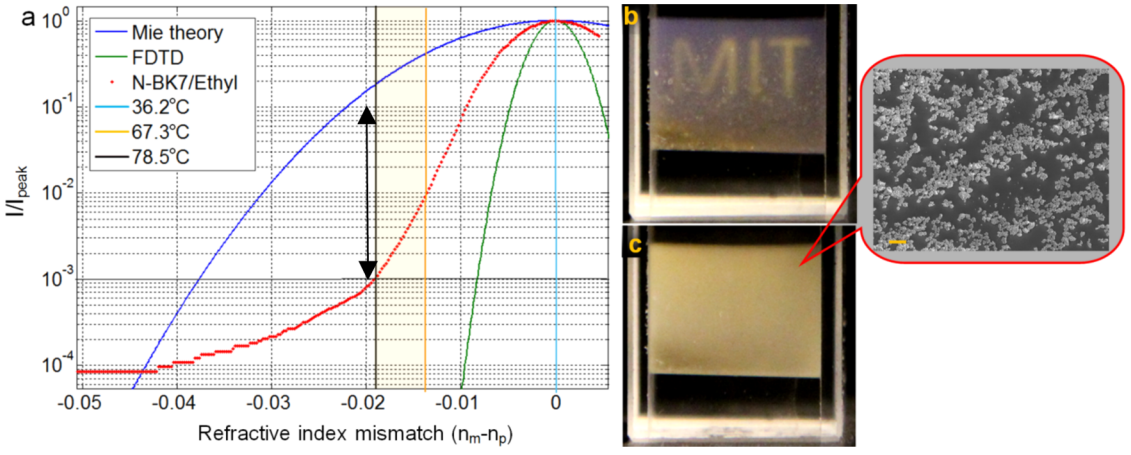

Figure 2. Experimental demonstration of Tyndall windows. (a) Transmission of the mixture. Red dots are the measurement data points, blue curve is prediction based on Mie theory and green curve is obtained by using FDTD simulation of packed particles. The graph is normalized to the peak (absorption is neglected). The measurements shows 2 orders of magnitude sharper transition, as shown by arrow. (b) The mixture is rendered transparent in the entire visible range, and the letters are readable at the back of the cuvette (c) The mixture has become diffusive again and the letters cannot be seen anymore. The inset figure shows the SEM image of N-BK7 glass particles used in the mixture. The scale bar is 5 μm.

scattering efficiency of a single particle hits zero (Figure 1 b) where the fwhm of this window is affected by particle size. The scattering coefficient can be calculated for spherical particles in the Mie scattering regime using a combination of first kind spherical Bessel functions and spherical Hankel functions,[21] as in eq 1.

$$\mu_s' = \frac{3fQ(m, k, a)}{4a}(1 - g(m, k, a)) \quad (1)$$

Here f is the volume fraction, k is the wave vector, a is the Mie particle radius, g is the scattering anisotropy function, and Q is the scattering efficiency function (for details of these functions, see Supplementary Note 1 in the Supporting Information (SI)). Figure 1d shows what the Tyndall window looks like as a function of refractive index mismatch and particle size relative to wavenumber.

At Tyndall window, the mean free path tends toward infinity, and therefore, the medium is not optically diffusive anymore, since the $\mu'_s \gg \mu_a$ assumption for the diffusion equation is no

DOI: 10.1021/acsphotonics.6b00199
ACS Photonics 2016, 3, 930–935

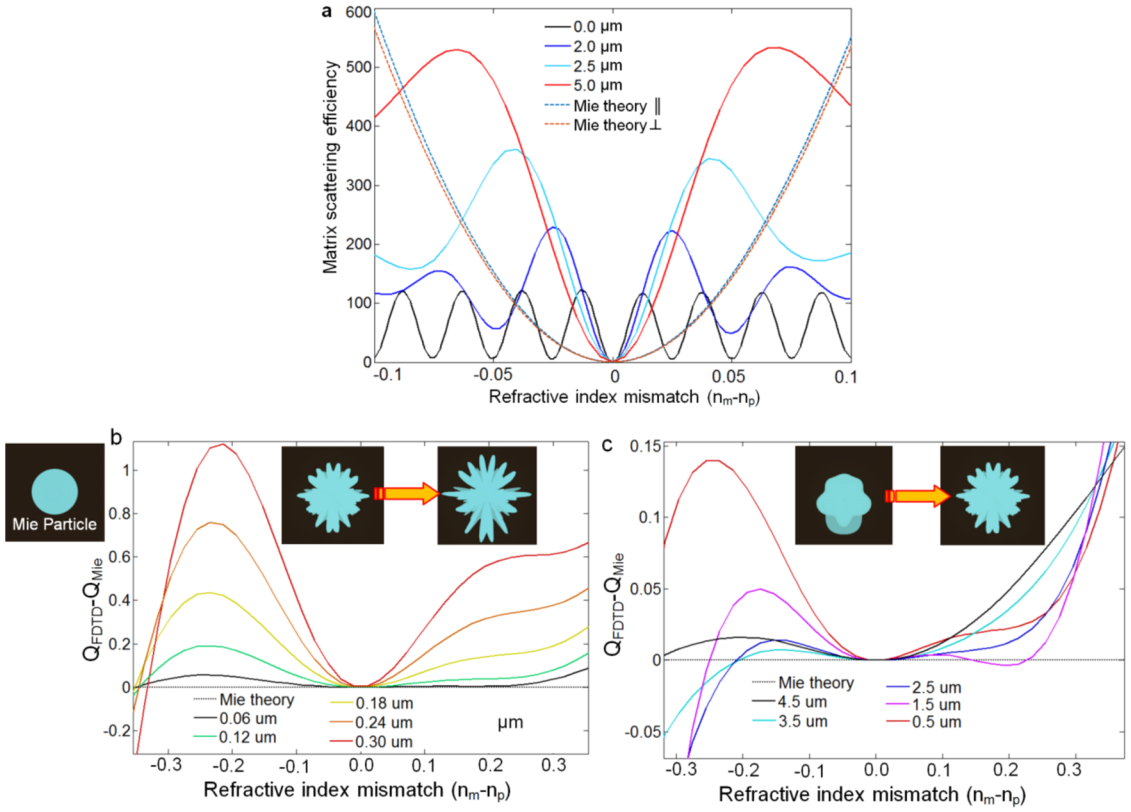

Figure 3. Particle packaging and roughness effects in Tyndall scattering. (a) Total scattering of a 30 × 30 matrix of particles with constant number of identical particles and different average distances. Scattering efficiency is notably sharper than what Mie theory predicts for smaller average distances. (b) Particle roughness amplitude effect on scattering. Inset image on the left corner shows a simple Mie particle. The particle is changed to Tyndall particle, and the amplitude of roughness is changed. (c) Scattering efficiency divergence from Mie theory when roughness frequency is changed. Inset figure shows a typical geometry change by change in the frequency of the roughness.

longer valid. At this point, the medium is completely transparent and the transmission ratio $I/I_0 = e^{-\mu' s d}$ reaches the maximum. Here I_0 is the input intensity, I is the output intensity, d is the distance that light travels in the mixture, and μ'_s is the scattering cross section, as in eq 1. The scattering cross section has significant modulation in amplitude in the Tyndall window where the scattering resonance is present. Aside from the refractive index ratio ($m = n_p/n_m$), the modulation depends on the size of the particles, as in Figure 1d.

While Figure 1d shows the concept clearly, the behavior is rather counterintuitive on the particle size axis as it is expected that the scattering would be less for smaller particles. This intuition is correct for a single particle; however, by considering the RTE for a large number of particles it is found that the overall transmission window will broaden for larger and smaller particles as predicted in Figure 1d. The asymmetry across the center of the maximum is due to anisotropy of scattering for Mie particles (for details, see Supplementary Note 1 (SI)).

The scattering efficiency Q_s and the scattering anisotropy g are infinite series as in Supplementary Note 1 (SI). The sum over l can be restricted to a few terms N. The proposed value by Bohren and Huffmann for N, $N = x + 4x^{0.5} + 2$, with $x = ka$ is used[22] in our calculations.

RESULTS

Figure 2a–c shows our measurement for a mixture of N-BK7 particles (~1 μm average diameter size) mixed in ethyl salicylate. The transmitted peak intensity for 655 nm laser beam passing through 2 mm of this mixture is modulated by about 3 orders of magnitude with 42 °C change in the temperature and an order of magnitude by only 11.2 °C from 67.3 to 78.5 °C. As a result of such modulation, the mixture can go from completely opaque to transparent, as in Figure 2b,c (see supplementary video (SI)).

It must be noted that this change in transmission peak is not due to a change in absorption, as the mixture absorption is almost constant and negligible for the entire temperature range. Therefore, this change in the intensity is directly indicative of the change in optical diffusion.

Figure 2a shows the normalized transmission of the mixture; the absolute total transmission of the input light through the entire cuvette is measured to be 35.8%. Therefore, the absolute peak transmission of the mixture is estimated as ~41% considering the 87.2% transmission of UV-fused quartz cuvette at 655 nm. The diffusion theory assumes no absorption and optical extinction for the medium; therefore, the probability of the scattered photons after distance d is $1 - \frac{I}{I_0} = 1 - \exp(-\mu_s' d)$, which in turn represents the cumulative distribution function of an exponential distribution with mean $l_s = 1/\mu'_s$. This parameter, also known as mean free path, is essential in biomedical applications[23] and can be estimated based on transmission measurements. For example, the mean free path due to Mie or in our case Tyndall scattering is estimated as $2.2 \times 10^{-3} m$ at peak transmission (36 °C), $3.6 \times 10^{-4} m$ at 67 °C, and $2.6 \times 10^{-4} m$ at 78 °C. Comparing these with $\sim 3.5 \times 10^{-4} m$ mean free path length for gelatin-TiO_2 tissue phantom[23] confirms that our mixture favorably covers the practical l_s range

DOI: 10.1021/acsphotonics.6b00199
ACS Photonics 2016, 3, 930–935

expected for tissue phantoms. In theory, at peak transmission, the mean free path tends toward infinity; however, we do not directly observe that due to impurities in the mixture and increase in inaccuracy of the diffusion model as the mixture goes toward peak transparency.

We find that by using Mie theory for particles of 1 μm and volume fraction of 0.74 (which is the maximum theoretical filling factor for spherical particles) the theoretical prediction curve (blue curve in Figure 2a) is yet much broader than our measurement (red dots in Figure 2a). Such sharp variations in measurements is especially unexpected since unlike polymer beads there is no chemical transition phase change or deformation for glass in such low temperatures.[5]

The sharpening of the transparency window can be attributed to two effects; packaging of the particles that can affect the mutual near-field effects and irregularities of the particles themselves that can create broader angular scattering of the light. Both of these factors are not captured by Mie theory. We used 2D FDTD simulation to capture these two effects. To capture the near-field effects we made a 30 × 30 matrix of identical 1 μm diameter particles that are distributed with uniform random distributions within each unit cell. There is only one particle in each unit cell of this matrix.

In the vicinity of the refractive index match, the scattering efficiency can be approximated as a parabolic function $Q \propto \Delta n^2$. As in Figure 3a, for smaller average distance, the packaging is tighter and the slope of the parabolic function becomes larger, and thus, ultimately, a smaller refractive index mismatch is needed for a given intensity modulation.

The oscillations in theses curves are because of the fact that we are considering a periodic unit cell structure along with identical particles. For example, in the case of zero average distance (the black curve in Figure 3a), the matrix will become like a photonic crystal, and therefore, the structure is completely periodic as the start point and end point of the uniform random distribution range is pushed toward a single point. This reduces the total scattering and also causes a periodic behavior.

An increase in scattering is also expected by increase in roughness. For studying roughness we used 2D Lumerical roughness model with sinusoidal preferential geometry, as in Figure 3c,d. We changed two parameters the roughness amplitude Figure 3b and frequency Figure 3c.

As noted the divergence from Mie theory increases nonlinearly and nonmonotonically for larger refractive index mismatch. However, the deviation close to matching point is not significant. This might be attributed to the small refractive index step at the liquid−particle interface that reduces the field perturbations at the particle boundary. The inset figures show how the geometry of the 2D Mie particle is changed by changing the roughness parameters. In the real experiment both of the effects are present simultaneously (inset image in Figure 2c). It is extremely computationally intensive to simultaneously capture both of the effects via FDTD even in 2D. This is because the roughness of individual particles requires finer subwavelength mesh and the volume fraction of the particles forces a larger simulation area.

DISCUSSION

At the Tyndall window the optical diffusion coefficient D peaks to infinity (Supplementary Note 2 (SI)), and the mixture becomes transparent. As the mixture exits the window, the medium becomes diffusive again and the fwhm diffusion angle is increased roughly quadratically with temperature (Figure 4). The dynamics of the diffusion coefficient is discussed further in

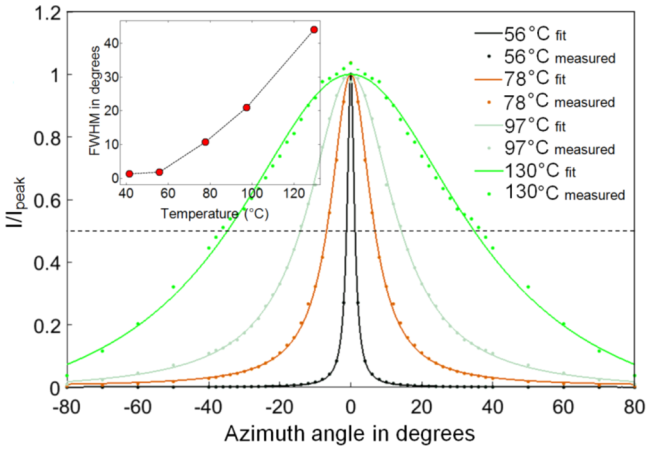

Figure 4. Measured diffusion angle for different temperatures. Angular intensity profile was measured to estimate the diffusion angle at different temperatures. Inset figure shows the fwhm for different temperature profiles extracted from the mathematical fit to the measurements in the main figure.

Supplementary Note 2 (SI). This tunable diffusion angle is especially valuable as more cumbersome material developments have been proposed to develop even single angle diffusers.[24] Specifically, the presence of Tyndall windows for glass-based materials promises a new tunable dimension for devitrite nanocrystals-based optical diffusers[24] and disordered photonics.[1]

In this work we used irregular glass particles to demonstrate the concept and frame the theory; however, polymer beads can also be carefully fabricated in large numbers to tune into a specific desired size.[5,10,25] One of the drawbacks for using polymers in our study though was the chemical phase transition of the polymers themselves (e.g., Nypam) that would have interfered with our study. The particles in the mixture can also be designed to have resonant scattering or specific directional character which is out of the scope of this work.[5,24,26,27]

In summary, the Tyndall window effect deepens the contrast or dichotomy between the small refractive index changes of the two materials in the mixture based on near-field effects and aggregation of random scattering from a volume of Tyndall particles. While the major trend can be predicted with conventional Mie theory, we find a notable divergence (over 2 orders of magnitude at some mismatch points) from Mie theory based on our measurements and FDTD results. The effect is purely due to difference in refractive index gradients of the two materials, therefore, it can be broadband and it is present in case of other external factors that modulate the refractive index. One such factor can be a secondary external electric field or an acoustic field. Near-field effects are not exploited in matching media. We expect this work to be applicable to a large class of future mixtures with different external triggers; for example, a mixture of photorefractive particles suspended in a matching liquid can result in an optically tunable Tyndall window.

Unlike the diffusion modulation depth that is notably increased due to a matching medium, the modulation speed is directly tied to the refractive index modulation speed of the individual components and is thus left intact. Since the

DOI: 10.1021/acsphotonics.6b00199
ACS Photonics 2016, 3, 930−935

containing medium is liquid, the mixture can be used as a tunable fluid phantom for optofluidics,[15] phase contrast microscopy,[27,28] optical flow-cytometry,[16] and rheology studies.[12] In a static form a larger volume of such a mixture might be considered as a tissue phantom with tunable scattering for biomedical studies. Tyndall windows indicate the great potential of combining matching media with near-field effects, these two elements can provide a platform for future nano-optic and micro-optic device engineering.

METHODS

To measure this effect we used a standard transmission measurement setup composed of a 0.7 mL, 2 mm quartz cuvette placed in front of a Gaussian beam emitted from a 100 mW, 655 nm CW laser diode (Dragon Lasers M series), the beam peak was fed into a photodiode (Thorlabs, model: DET36A). The voltage of the photodiode was measured with an oscilloscope (Tektronix, model: TDS 2024B). Furthermore, for the noise elimination two pinholes were used to block any scattered light from the cuvette or surroundings and a long pipe was shielding the photodiode. The sample inside the cuvette was heated up with a hot plate (Corning, model: PC-400D) to 195 °C. While cooling down to room temperature the temperature of the cuvette was measured using a noncontact IR temperature gun.

Ethyl salicylate is a clear optical liquid sometimes used in flavoring and perfume industries. Due to the absence of polarity of its molecules it has a linear temperature variation which can be described by the following function: $\Delta n = n_0 + n_1 T$. Here T has units of Kelvins.[29] The coefficient n_0 and n_1 were obtained by fitting the literature value for ES at various temperatures to be $n_0 = 1.636$ and $n_1 = -0.0004497$.[30] A property of borosilicate present in N-BK7 glass is its low thermal expansion coefficient which leads to very small temperature dependence refractive index change.[17] We used the McCone micronizing mill to produce glass microparticles used in the experiment. The process is fully mechanical and thus leaves some impurities in the mixture even after sonication and non invasive chemical wash.

FDTD simulations were performed with Lumerical software. For the irregular particle shape a rough surface is characterized by an RMS amplitude and a correlation length. Lumerical uses a computational strategy to avoid an abrupt seam when wrapping the rough surface to create the cylindrical shape.

For the near-field effect simulation the perfectly matched layer (PML) boundary condition were used. It was assumed that the materials are nonabsorbing. For monitoring the scattering we used a total-field- scatter-field (TFSF) monitor. Polarization does not play a notable part as the particles are random and do not have a specific anisotropic geometry in our study. Polarization of the input light for 2D FDTD simulations was perpendicular to the plane of the simulations (parallel to the cylinder axis).

ASSOCIATED CONTENT

Supporting Information

The Supporting Information is available free of charge on the ACS Publications website at DOI: 10.1021/acsphotonics.6b00199.

(Supplementary note 1) Theoretical framework used for anisotropic Mie scattering estimation versus refractive index mismatch. (Supplementary note 2) More details on optical diffusion dynamics and diffusion angle measurement geometry (PDF).

Supplementary video (MP4).

AUTHOR INFORMATION

Corresponding Author

*E-mail: barmak@mit.edu.

Notes

The authors declare no competing financial interest.

ACKNOWLEDGMENTS

The authors like to acknowledge intellectual support from Prof. Federico Capasso at Harvard University, technical assistance from Dr. Mark Wilson and Prof. Moungi Bawendi, and also technical assistance for sample preparation from Poorya Hosseini, Carole Lucie Gadois, Gita Kiaee, and Prof. Antoine Allanore at Massachusetts Institute of Technology.

REFERENCES

(1) Wiersma, D. S. Disordered Photonics. *Nat. Photonics* **2013**, *7*, 188−196.

(2) Graydon, O. Photochromic Materials: Switchable Absorber. *Nat. Photonics* **2014**, *8*, 499−499.

(3) Zhu, J.; Kim, W. J.; He, G. S.; Seo, J.; Yong, K.-T.; Lee, D.; Cartwright, A. N.; Cui, Y.; Prasad, P. N. Enhanced Photorefractivity in a Polymer/nanocrystal Composite Photorefractive Device at Telecommunication Wavelength. *Appl. Phys. Lett.* **2010**, *97*, 263108.

(4) Krebs, F. C. Electrochromic Displays: The New Black. *Nat. Mater.* **2008**, *7*, 766−767.

(5) Seeboth, A.; Ruhmann, R.; Mühling, O. Thermotropic and Thermochromic Polymer Based Materials for Adaptive Solar Control. *Materials* **2010**, *3*, 5143−5168.

(6) Gelinck, G. H.; Huitema, H. E. A.; van Veenendaal, E.; Cantatore, E.; Schrijnemakers, L.; van der Putten, J. B. P. H.; Geuns, T. C. T.; Beenhakkers, M.; Giesbers, J. B.; Huisman, B.-H.; Meijer, E. J.; Benito, E. M.; Touwslager, F. J.; Marsman, A. W.; van Rens, B. J. E.; de Leeuw, D. M. Flexible Active-Matrix Displays and Shift Registers Based on Solution-Processed Organic Transistors. *Nat. Mater.* **2004**, *3*, 106−110.

(7) Terentjev, E. Liquid Crystals: Interplay of Topologies. *Nat. Mater.* **2013**, *12*, 187−189.

(8) Talarico, M.; Golemme, A. Optical Control of Orientational Bistability in Photorefractive Liquid Crystals. *Nat. Mater.* **2006**, *5*, 185−188.

(9) Sell, J. *Photothermal Investigations of Solids and Fluids*; Elsevier Science, 2012.

(10) Seeboth, A.; Kriwanek, J.; Vetter, R. The First Example of Thermochromism of Dyes Embedded in Transparent Polymer Gel Networks. *J. Mater. Chem.* **1999**, *9*, 2277−2278.

(11) Reufer, M.; Díaz-Leyva, P.; Lynch, I.; Scheffold, F. Temperature-Sensitive poly(N-Isopropyl-Acrylamide) Microgel Particles: A Light Scattering Study. *Eur. Phys. J. E: Soft Matter Biol. Phys.* **2009**, *28*, 165−171.

(12) Lee, H.; Shin, Y.; Kim, S. T.; Reinherz, E. L.; Lang, M. J. Stochastic Optical Active Rheology. *Appl. Phys. Lett.* **2012**, *101*, 31902.

(13) Hajjarian, Z.; Nadkarni, S. K. Estimation of Particle Size Variations for Laser Speckle Rheology of Materials. *Opt. Lett.* **2015**, *40*, 764−767.

(14) Schmidt, H.; Hawkins, A. R. The Photonic Integration of Non-Solid Media Using Optofluidics. *Nat. Photonics* **2011**, *5*, 598−604.

(15) Fan, X.; White, I. M. Optofluidic Microsystems for Chemical and Biological Analysis. *Nat. Photonics* **2011**, *5*, 591−597.

(16) Wong, T. T. W.; Lau, A. K. S.; Ho, K. K. Y.; Tang, M. Y. H.; Robles, J. D. F.; Wei, X.; Chan, A. C. S.; Tang, A. H. L.; Lam, E. Y.; Wong, K. K. Y.; Chan, G. C. F.; Shum, H. C.; Tsia, K. K. Asymmetric-

DOI: 10.1021/acsphotonics.6b00199
ACS Photonics 2016, 3, 930−935

Detection Time-Stretch Optical Microscopy (ATOM) for Ultrafast High-Contrast Cellular Imaging in Flow. *Sci. Rep.* **2014**, *4*, 3656.
(17) Liebetraut, P.; Waibel, P.; Nguyen, P. H. C.; Reith, P.; Aatz, B.; Zappe, H. Optical Properties of Liquids for Fluidic Optics. *Appl. Opt.* **2013**, *52*, 3203−3215.
(18) Zhou, S.; Fan, S.; Au-yeung, S. C. F.; Wu, C. Light-Scattering Studies of poly(N-Isopropylacrylamide) in Tetrahydrofuran and Aqueous Solution. *Polymer* **1995**, *36*, 1341−1346.
(19) Wang, L. V.; Wu, H.-I. *Biomedical Optics*; John Wiley & Sons, Inc.: Hoboken, NJ, U.S.A., 2009.
(20) Rheims, J.; Köser, J.; Wriedt, T. Refractive-Index Measurements in the near-IR Using an Abbe Refractometer. *Meas. Sci. Technol.* **1997**, *8*, 601−605.
(21) Cox, A. J.; DeWeerd, A. J.; Linden, J. An Experiment to Measure Mie and Rayleigh Total Scattering Cross Sections. *Am. J. Phys.* **2002**, *70*, 620.
(22) Bohren, C. F.; Huffman, D. R. *Absorption and Scattering of Light by Small Particles*; Wiley-VCH Verlag GmbH: Weinheim, Germany, 1998.
(23) Akarçay, H. G.; Preisser, S.; Frenz, M.; Rička, J. Determining the Optical Properties of a gelatin-TiO(2) Phantom at 780 Nm. *Biomed. Opt. Express* **2012**, *3*, 418−434.
(24) Butt, H.; Knowles, K. M.; Montelongo, Y.; Amaratunga, G. A. J.; Wilkinson, T. D. Devitrite-Based Optical Diffusers. *ACS Nano* **2014**, *8*, 2929−2935.
(25) *Scattering Methods and the Properties of Polymer Materials*; Springer Science & Business Media, 2005.
(26) Wu, H.-J.; Shah, S.; Beckham, R.; Meissner, K. E.; Bevan, M. A. Resonant Effects in Evanescent Wave Scattering of Polydisperse Colloids. *Langmuir* **2008**, *24*, 13790−13795.
(27) Chibani, H.; Dukenbayev, K.; Mensi, M.; Sekatskii, S. K.; Dietler, G. Near-Field Scanning Optical Microscopy Using Polymethylmethacrylate Optical Fiber Probes. *Ultramicroscopy* **2010**, *110*, 211−215.
(28) Ford, T. N.; Chu, K. K.; Mertz, J. Phase-Gradient Microscopy in Thick Tissue with Oblique Back-Illumination. *Nat. Methods* **2012**, *9*, 1195−1197.
(29) Sheu, Y. W.; Tu, C. H. Densities, Viscosities, Refractive Indices, and Surface Tensions for 12 Flavor Esters from T = 288.15 K to T = 358.15 K. *J. Chem. Eng. Data* **2005**, *50*, 1706−1710.
(30) Ghosh, G.; Endo, M.; Iwasaki, T. Temperature-Dependent Sellmeier Coefficients and Chromatic Dispersions for Some Optical Fiber Glasses. *J. Lightwave Technol.* **1994**, *12*, 1338−1342.

DOI: 10.1021/acsphotonics.6b00199
ACS Photonics 2016, 3, 930−935